Understanding the process of lithium deposition on a graphite anode for better lithium-ion batteries

XU Yu-jie[1,†], WANG Bin[1,†], WAN Yi[1], SUN Yi[1], WANG Wan-li[1], SUN Kang[2], YANG Li-jun[3], HU Han[1,*], WU Ming-bo[1,*]

（1. *College of Chemistry and Chemical Engineering*, *College of New Energy State Key Laboratory of Heavy Oil Processing*, *China University of Petroleum (East China)*, *Qingdao* 266580, *China*;
2. *Institute of Chemical Industry of Forest Products*, *Chinese Academy of Forestry*, *Nanjing* 210042, *China*;
3. *Qingdao Guanbaolin Activated Carbon Co.*, *Ltd.*, *Qingdao* 266313, *China*）

Abstract: A brief overview of recent developments in the formation, detection, and suppression of lithium dendrites in carbon-based lithium-ion batteries is presented. The electrochemical processes that result in the formation of lithium dendrites on the anode surface are reviewed, and various detection methods, including the essential operando technique for understanding the complex mechanism, are then introduced. Methods for suppressing lithium dendrite formation are discussed and prospects for future research and development are presented.

Key words: Graphite anode; Lithium deposition; Lithium-ion batteries; Mechanism; In situ detection

1 Introduction

Since the advent of the 21st century, the utilization of fossil fuels and other non-renewable energy sources has rapidly declined due to the rapid growth of industrial and agricultural sectors[1–2]. Therefore, it is imperative to explore and effectively implement new renewable energy to alleviate the strain on energy demand, preserve finite non-renewable resources, and ensure the continuation of normal human production and lifestyles[3–4]. Furthermore, the call for "Carbon Neutrality" has led to a significant surge in research and development of new energy vehicles that prioritize long endurance and high safety, with electrochemical energy storage devices being the preferred power source for these vehicles[5]. Additionally, in order to fully electrify the transportation sector, it is crucial to prioritize research and development and the promotion of electric vehicles. Two of the most important challenges in this effort include increasing the driving life of these vehicles and implementing fast charging technology.

Lithium-ion batteries (LIBs) are widely recognized as a hallmark of electrochemical energy storage technology and are considered the most suitable power source for portable electronic devices due to their high energy density, long cycle life and low self-discharge rate[2, 6–8]. LIBs consist of a cathode, an anode, separators, current collectors and electrolytes[9–10]. Redox reactions can occur spontaneously at both electrodes, which releases electrons and generates an output current when the two electrodes are connected externally[11].

Graphite, a carbon-based material, is commonly used as the anode in LIBs. Graphite comprises ABAB layers held together by van der Waals forces, within each layer the carbon stomes are connected by sp^2 bond[12]. At room temperature, the capacity of graphite as a lithium-ion anode is limited by the fact that only one lithium ion can intercalate into hexatomic carbon ring, resulting in a stoichiometry of LiC_6. This results in a theoretical capacity of 372 mAh g^{-1}, which is significantly lower compared to that of lithium metal anode (3 860 mAh g^{-1})[13–14]. While the formation of micro-structured lithium dendrites during the charging and discharging process in the lithium metal anode can lead to internal short-circuiting within the

Received date: 2023-03-01; **Revised date:** 2023-04-28

Corresponding author: HU Han, Professor. E-mail: hhu@upc.edu.cn;
WU Ming-bo, Professor. E-mail: wumb@upc.edu.cn

Author introduction: XU Yu-jie† and WANG Bin† contributed equally to this work.

cell, causing serious safety concerns[15]. In comparison, the advantages of graphite, including its high electrical conductivity, low cost, long cycle life, low swelling and good safety, have ensured its status as the most commonly used anode material.

Despite its advantages, there are still limitations and challenges associated with the use of graphite as the anode material in LIBs[16–18]. One major issue is the formation and growth of metallic lithium on the graphite anode, which is a side effect of Faradaic reactions[19]. The most recent review pertaining to the lithium planting on graphite surfaces was from Waldmann et al.[16]. However, over the past 5 years, various techniques have rapidly developed, particularly novel *in-situ* techniques, which are expected to deepen the understanding of lithium deposition behaviors. As such, it is necessary to draft a review that comprehensively summarizes the recent progress in this field. Thus, this review will address the challenges faced by graphite materials as anodes in LIBs by discussing the basic electrochemical processes that occur on their surface. To effectively avoid lithium deposition and understand the timing, location, and causes of it, advanced characterization methods for the deposition process are introduced. The review also examine the factors that influence the occurrence of lithium plating and methods that inhibit the lithium plating.

2　Basic electrochemical processes on graphite anode

The graphite anode undergoes 3 basic electrochemical processes during charge/discharge (Fig. 1). The first process, solid electrolyte interface (SEI) formation, occurs during the first cycle of the battery. This is when a thin layer of lithium salts forms on the surface of the graphite anode, which acts as a barrier between the anode and the electrolyte. The SEI layer helps to reduce the leakage of Li^+ into the electrolyte and prevent the formation of a direct lithium metal anode, which causes short-circuiting and other safety issues. The second process, the reversible intercalation of Li^+ into the interstitial spaces of the graphite layers and the extraction of these ions during the battery's

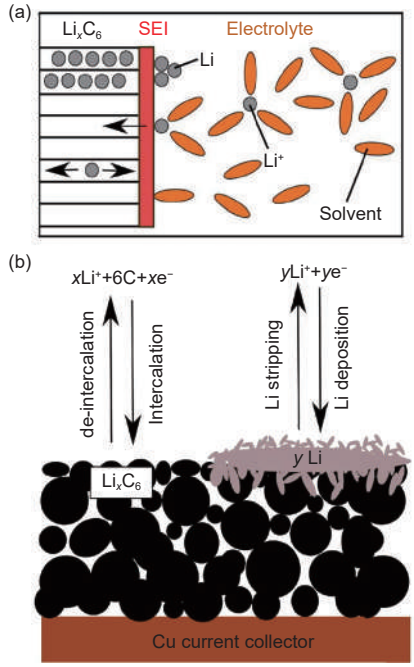

Fig. 1　(a) Mechanism for the SEI formation. (b) Possible electrochemical processes occurred on graphite anode under the microscopic level[16]. Reproduced with permission. Copyright 2018, Elsevier B.V.

discharge and charge cycle. This process results in a change in the volume of the graphite anode, which causes mechanical stress and affect the battery's life cycle. What's more, the low Li^+ diffusivity in the graphite layer (approximately 10^{-7} cm^2 s^{-1}) hinders the fast Li^+ migration and makes it difficult to achieve high rate capability[20]. Finally, the third process, lithium deposition, is a result of a side effect from the Faradaic reaction. The formation of a micro-structured lithium layer can increase the risk of short circuits, thermal runaways, and even battery explosions[16, 18].

The lithium insertion and deposition potentials are not thermodynamically competing. The insertion potential is around 0.2 V *vs*. Li^+/Li, while the deposition potential is below 0 V[21]. Despite this, polarization caused by factors such as ohmic drop, diffusion overpotential and charge transfer overpotential is the main contributor to lithium deposition, making it a complex process. There are 2 theoretical models for Li^+ deposition: one is based on the critical saturation concentration of lithium ions and the other is based on the interface overpotential.

Landau et al.[22] proposed that during the char-

ging process, a concentration gradient of Li^+ is created at the graphite/electrolyte interface due to the fact that the rate of Li^+ transport at the SEI interface is typically greater than the diffusion rate of Li^+ between the graphite layers. As a result, the charging process is governed by mass transport, leading to the enrichment of Li^+ at the graphite anode, and the occurrence of lithium plating at a concentration of 0.077 mol cm^{-3}.

Arora et al.[23] presented a proposal for the deposition of lithium on porous anodes, which is based on the Doyle-Fuller-Newman model. This model encompasses both the current of Li^+ that have been inserted, as well as the current of plated Li^+, and the Butler-Volmer equation establishes a connection between the current and the potential of the lithium deposition reaction. The proposed setpoint for lithium deposition in the model by Arora et al. was a voltage below 0 V *vs*. Li^+/Li.

Subsequently, Tang et al.[24] expanded upon the Arora's model by extending it to a two-dimensional framework in order to examine the impact of the edge interface on electro-deposition. Furthermore, Perkins and colleagues[25] simplified the Arora model through the use of the Poisson reduction technique, preserving the precision of the original model while reducing the computational load.

Overall, the design of the battery, performance of the materials, and operating conditions play crucial roles in affecting the deposition of lithium on graphite anode[16–18, 24]. From a battery level, the ratio of capacity between the anode and cathode is critical[23–24]. It is generally considered optimal to have the anode capacity exceed that of the cathode in order to ensure that the lithium insertion into graphite remains below 100% State of Charge (SOC). As the SOC has a significant impact on the diffusion rate of Li^+ within the graphite layer[26–27]. For example, the diffusion rate of Li^+ tends to decrease at higher SOC. Additionally, the geometric configuration of the anode and cathode, as well as the thickness of the separator, also play a role in lithium plating. Simulation results demonstrate that extending the length of the graphite sheet (to 0.4 mm) and increasing the thickness of the separator could effectively mitigate lithium plating[23,28]. From a dynamic standpoint, the formation of dendrites is dependent on the movement of Li^+ within the anode pores. The factors such as the particle size, surface roughness and shape of the anode material can have an impact on the formation of dendrites. Operating conditions, including temperature and charge-discharge current density, also play a critical role in the formation of dendrites[27, 29–33]. For instance, low temperatures reduce the diffusion rate of Li^+ between layers, whereas high current densities increase the ionic flux through the SEI layer, leading to a heightened concentration of Li^+ at the graphene interface and eventual dendrite formation.

3 Detecting deposited lithium on graphite anode

Operando methods are experimental techniques that allow for the measurement of chemical and physical changes in a material during its operation, or while a process is taking place. Thus, operando methods are essential for understanding the complex mechanisms of lithium deposition on graphite anodes, identifying the factors that promote dendrite formation and growth, and developing effective strategies to mitigate these issues. For example, optical microscopy, nuclear magnetic resonance (NMR), electron paramagnetic resonance (EPR) and neutron reflectometer (NR) have been developed to investigate the planting behaviors. The insights gained from operando studies can inform the development of new battery materials and designs that are more durable, efficient and safe.

The addition of a reference electrode is the most efficient way to detect the real potential of the graphite anode to determine the electrodeposition process of metallic lithium. When metallic lithium is introduced into the graphite/$LiCoO_2$ cell as a reference electrode, lithium deposition on the surface of graphite is frequently observed, particularly at low temperatures and high current densities during cycling (Fig. 2a)[34]. It has been found that exceeding a certain threshold cur-

rent (0.4 C in this case) does not reduce the charging time, but rather aggravates the lithium deposition.

To discern the occurrence of lithium plating during high-rate charging, it is possible to analyze differential voltage-capacity (dQ/dV) discharge curves. When lithium plating occurs (Fig. 2b), a distinct feature can be observed in the voltage curve, which corresponds to the stripping of lithium and the potential difference between lithium stripping and deintercalation from the negative electrode[35]. However, in order to accurately identify this feature in the differential voltage or differential capacity curves, a significant amount of lithium plating must have taken place. Specifically, by testing the open circuit voltage (OCV) of the battery at a certain time period after charging and analyzing the changes in its differential data, it is possible to detect the presence of lithium plating[36]. As shown in Fig. 2c, the initial relaxation voltage plateau represents a mixture of metallic lithium and Li_xC. As the metallic lithium continues to insert into the graphite layers, the potential continues to change until a new plateau appears when the plated lithium is exhausted and only the solid-phase Li_xC exists. This phenomenon is more clearly manifested in the differential OCV curve, which exhibits a peak. This testing method has been validated in terms of Coulombic efficiency (CE) and the detection limit was found to be 4 mAh plated Li per gram graphite.

The crystal structures of metallic lithium and graphite differ during lithium intercalation or deintercalation. These processes can be investigated separately through lateral or single-plane experiments. By utilizing an *in-situ* pouch cell and conducting microtomographic imaging experiments, it was able to determine the position of lithium plating and local strain inside the graphite electrode[37]. As shown in Fig. 3a, a polyether ether ketone (PEEK) battery holder was constructed for *in-situ* X-ray microtomography and segmentation. The lithium-graphite battery which has been charged to desired SOC was imaged in various charge states using a 10× lens and a 22 keV monochromatic beam. Strain calibration with respect to the SOC was established by analyzing tomographic images acquired under extremely slow charging conditions (C/10). This study reveals that during rapid charging, a mossy lithium layer forms at the interface between the graphite electrode and the separator, causing transport barriers and leading to the detachment of un-intercalated graphite particles positioned directly beneath the mossy lithium layer (Fig. 3b). This implies that the phenomenon of lithium plating hinders further intercalation of the bottom layer of graphite particles in the electrode. The authors explained that due to the transport barriers caused by lithium plating, the salt concentration gradient inside the electrode becomes steep, thereby resulting in a potential lithium deficiency in the bottom particles of the graphite electrode and reduced intercalation levels[38–40].

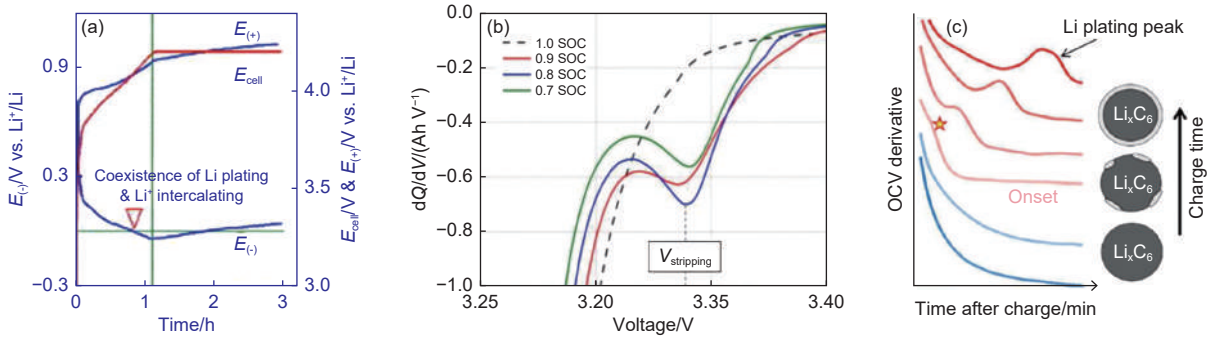

Fig. 2　(a) Cell voltage, cathode potential, and anode potential *vs*. charging time of a mesophase carbon micro beads (MCMB)/$LiCoO_2$ lithium-ion cell in typical CC/CV charging profiles[34]. Reproduced with permission. Copyright 2006, Elsevier B.V. (b) Differential capacity curves of the discharge profiles after charging to different SOC levels at −20 °C with 1 C charge current[35]. Reproduced with permission. Copyright 2013, Elsevier B.V. (c) Differential OCVs extracted from cycling data in cycles begin with fully delithiated graphite (x < 0.01 in Li_xC_6), which is ensured by slow C/5 discharging up to 1.5 V. After 4 C charging to 25%–40% SOC, the dQ/dV profiles show an inflection point feature not observed at 15%–20% SOC, suggesting plating begins near 25% SOC[36]. Reproduced with permission. Copyright 2020, American Chemical Society

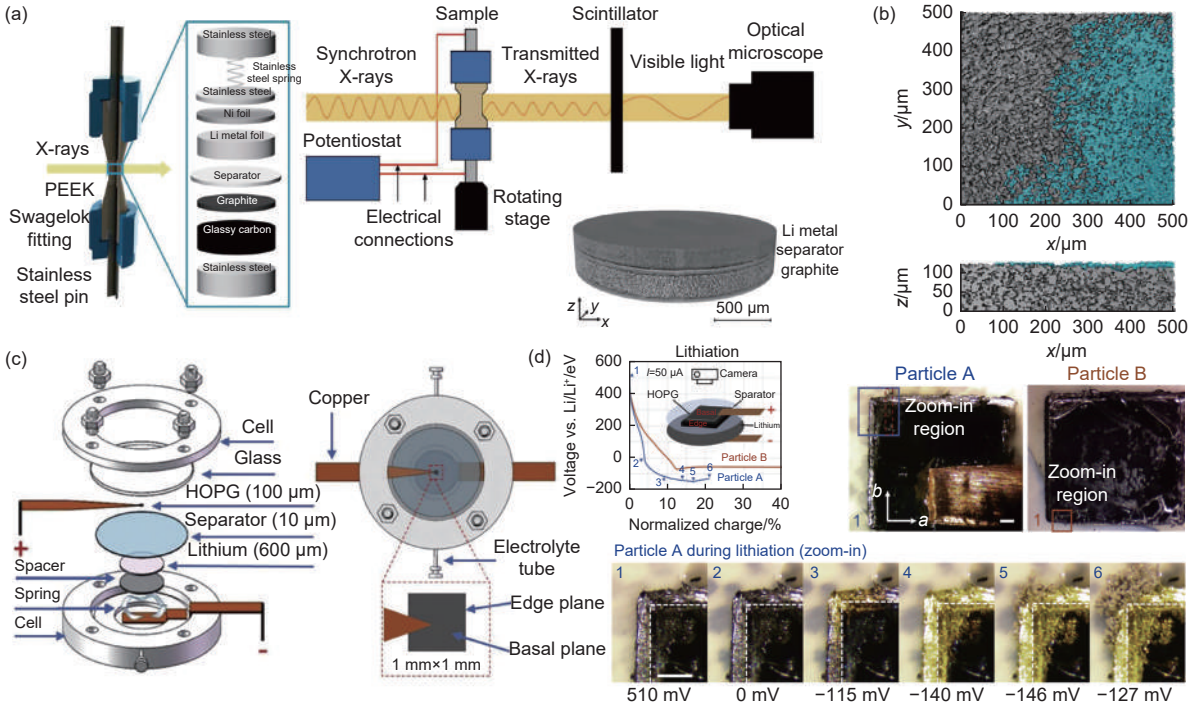

Fig. 3 (a) Schematics of the X-ray microtomography setup and cell configuration. (b) Volume rendering of the NW portion of the segmented graphite electrode in the xy-plane and xz-plane after discharge to 100% SOC at 1C. The gray indicates the graphite and the mossy lithium is shown in turquoise[37]. Reproduced with permission. Copyright 2021, American Chemical Society. (c) Schematic of the optical electrochemical *in-situ* cell. (d) Voltage profile and optical images of the HOPG under various potentials[40]. Reproduced with permission. Copyright 2021, Elsevier Inc

Gao et al.[40] then utilized the extracted concentration curve of embedded Li^+ and the total amount of lithium deposition on graphite particles to construct a physical image that describes the interplay between Li^+ embedding and deposition in graphite particles, as summarized in Fig. 3c-d. Single highly oriented pyrolytic graphite (HOPG) particles was chosen by them as the model system for the study with a custom *in-situ* electrochemical cell during cycling (Fig. 3c). The insertion of Li^+ into graphite layers is accompanied by a color change, which can be observed as a golden during the insertion process. The research findings indicate that the insertion of Li^+ starts from the edges and the kinetics of Li^+ intercalation into graphite layers is slow. Consequently, under high current conditions, foamy metallic lithium deposits start to form on the graphite surface (Fig. 3d). Additionally, a phase field model was developed to forecast the starting conditions of lithium deposition (Fig. 4). The findings indicate that the solid solution model is inadequate in predicting lithium deposition in graphite, as it typically underestimates the lithium concentration on the graphite surface.

To obtain more accurate predictions, a more precise phase transformation model is necessary. By using electrochemical calorimetry (Fig. 5a), it is possible to perform high-sensitivity *in-situ* detection of lithium deposition on the graphite electrode, as there are distinctive and identifiable thermal features in the heat flow at the beginning of the process[41]. Specifically, a small heat release was observed at the point where the battery is switched from discharge to charge, which corresponds to the small plateau in the battery voltage during lithium stripping resulting from the combined effect of entropy and the potential of the electrochemical cell. As such, the circular feature observed in the thermal spectrum can be attributed to the onset of lithium deposition and complete lithiation of the graphite structure.

Deposition of lithium on the negative electrode requires more space compared to intercalation compounds, resulting in an increase in the overall battery volume. Hence, the thickness variation during cycling can serve as a qualitative indicator for lithium

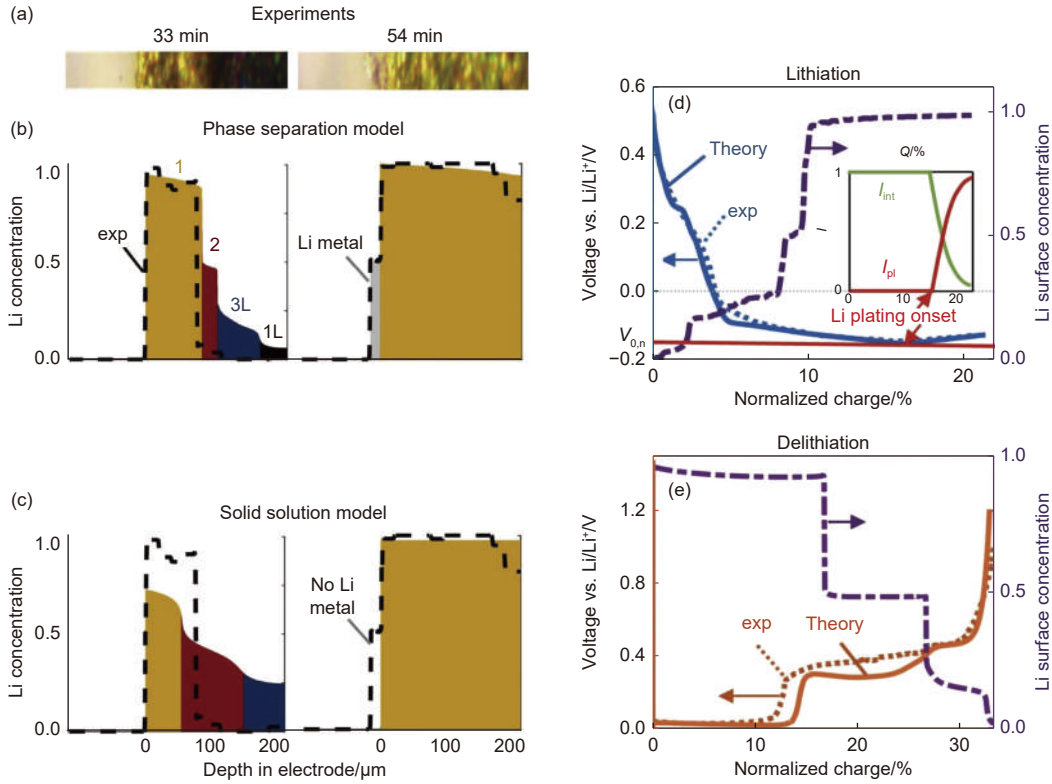

Fig. 4　(a) Examples of graphite particles images used to extract the lithium concentration and lithium plating profiles. (b) The phase separation model and the solid-solution model used to understand the lithium deposition processed. Voltage and the corresponding lithium surface concentration during (d) lithiation and (e) de-lithiation of graphite[40]. Reproduced with permission. Copyright 2021, Elsevier Inc

plating[42]. However, careful selection of the measurement location is required during testing since certain areas, such as the edge region, are more prone to plating. To assess the thickness variation caused by charging or plating accurately, researchers have developed a high-precision laser triangulation system with a resolution of micrometer scale (1.5 μm).

Acoustic ultrasonic (Fig. 5b) waves are also employed to detect the lithium planting in standard cells[43]. The acoustic flight time endpoint difference, which is defined by the acoustic flight time offset between the slow charge top and the fast electroplating-induced charge top, has been demonstrated as a promising parameter to determine the degree of lithium metal electroplating in the battery region connected to the acoustic transducer. From Fig. 5c, a statistically significant linear relationship has been identified between the ultrasonic flight time and graphite staging, as well as the acoustic flight time and post-mortem electrochemical measurements, to characterize the degree of lithium metal electroplating.

The lithium deposition in non-proton electrolytes can be tracked through the NR in specular reflectivity mode[44]. Analysis of the scattering length density (SLD) profile (Fig. 6a) obtained by modeling the reflectivity data clearly indicates that nm-thin lithium layers deposited above the SEI layer, which is initially formed, can be detected and their roughness can be estimated (Fig. 6b). This is a characteristic parameter of the non-uniformity of electrodeposition. Lithium plating can be determined in neutron diffraction by using LiC_{12} and LiC_6 because the contact between metallic lithium and graphite anode is unstable and results in lithium diffusion into the graphite (Fig. 6c)[45]. Compared with the slower C/5 reference cycle (Fig. 6c), neutron diffraction shows that the degree of lithium intercalation into graphite is lower after a sufficiently fast charging cycle, which is expected to result in significant lithium plating (C/30 charging rate). After 20 h of rest period following charging, the remaining LiC_{12} gradually transforms into LiC_6, indicating that lithium diffuses into the graph-

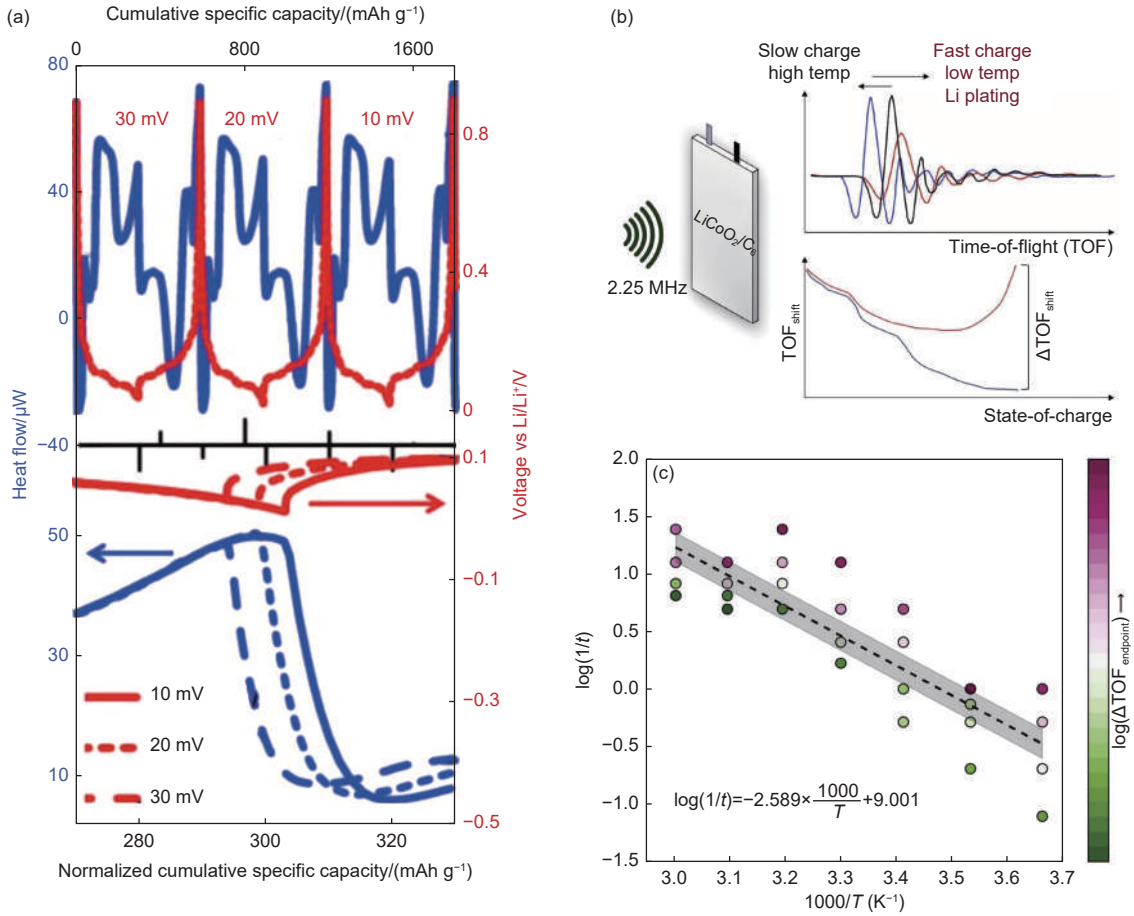

Fig. 5 (a) Thermal (blue) and voltage (red) profiles of a MCMB graphite/lithium half cell cycled at C/10 to varying cutoff voltages[41]. Reproduced with permission. Copyright 2013, The Electrochemical Society. (b) Linear relationships between ultrasonic time-of-flight (TOF) and graphite staging. (c) The relationship between the logarithmic rate (1/*t*) and the inverse temperature (1000/*T*), the color bar is used to factor in the TOF endpoint difference between the C/15 charge and the fixed capacity charge[43]. Reproduced with permission. Copyright 2020, Cell Press

ite (Fig. 6d).

NMR is utilized to directly measure metallic lithium. As summarized in Fig. 7a, the lithium ion signals in SEI and residual electrolyte have almost no chemical shift and are centered at a chemical shift of −4 ppm. A broad peak centered at −57 ppm is attributed to non-stoichiometric species of lithium distributed widely in graphite[46]. The intrinsic signal of metallic lithium appears at 247 ppm, and further analysis of the NMR spectra of surface lithium dendrites (270 ppm) and dense mossy lithium (261 ppm) can be differentiated (Fig. 7b-c)[47–48]. This model is further validated by the results of magnetization calculations and experimental NMR and scanning electron microscopy (SEM) data. The *in-situ* NMR battery developed by Grey can simultaneously monitor the performance of the cathode and anode[49]. Although metallic lithium was not detected in these batteries in the initial room temperature experiments, deposition of metallic lithium was observed at low temperatures (Fig. 7d). The deposition of metallic lithium after low temperature also occurred at 25 °C, which has never been reported before and is likely due to the accumulation of SEI and blockage of graphite pores where metallic lithium is formed at low temperature. These observation results indicate that even under so-called “safe” operation, the deposition of lithium at low temperatures will continue to accelerate capacity decay.

EPR can also be used to test the lithium metal situation in graphite anodes. The EPR signal of surface lithium metal in a conductive EPR spectrum is an asymmetric Dysonian line shape. The EPR signals of lithium metal, porous lithium metal and lithium dendrites are drastically different due to the effects of lithi-

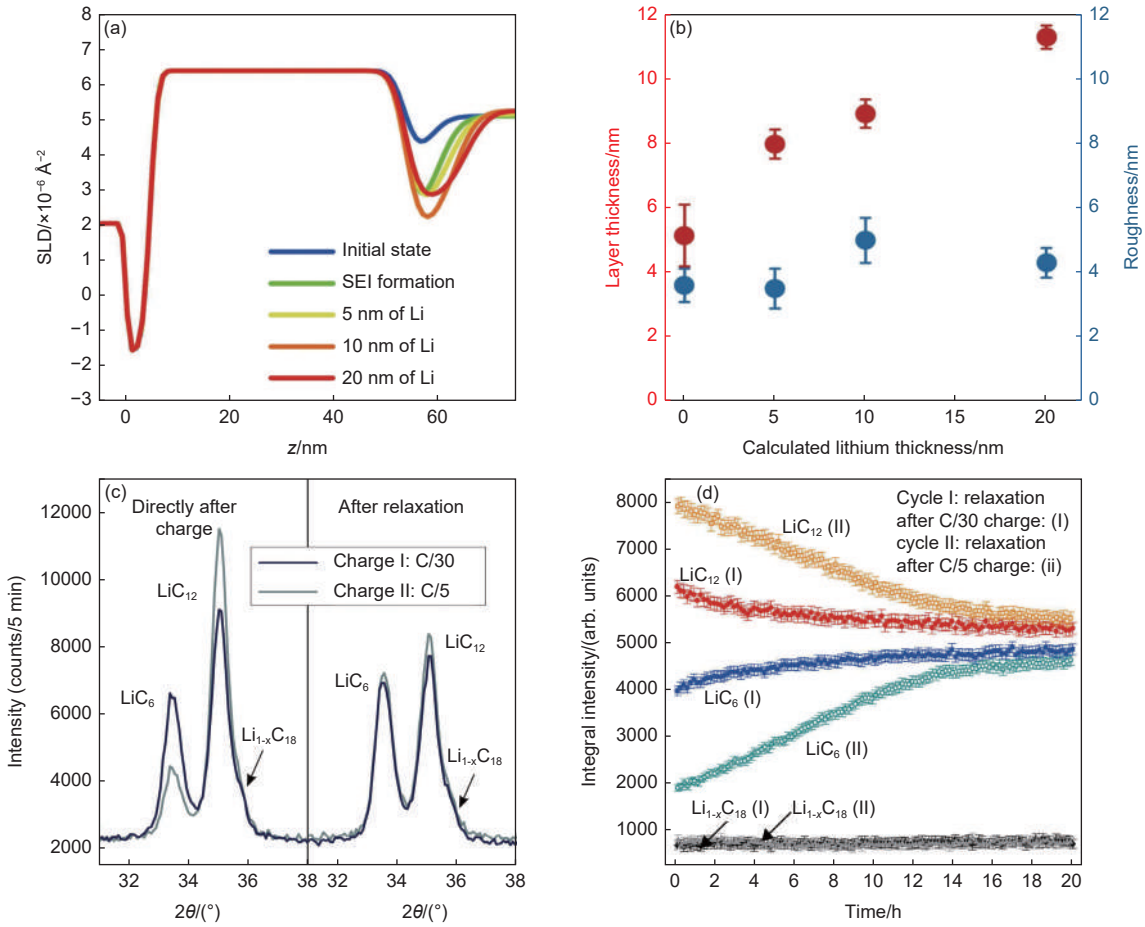

Fig. 6　(a) Fitting profiles of scattering length density (SLD) under different lithium layers. (b) Dependences of the mean thickness and roughness of the deposited layer (SEI + lithium) on the lithium layer thickness calculated from electrochemical data[44]. Copyright 2017, Elsevier B.V. (c) The diffraction data of the graphite anode under different conditions, which was charged at C/5 or C/30 charge (left) and after a 20 h relaxation period at −20 °C (right). (d) Changes of integral reflection intensity of LiC_{12} (red, orange), LiC_6 (blue, cyan) and $Li_{1-x}C_{18}$ (black, gray) during 20 h relaxation at −20 °C under C/30 and C/5 charge[45]. Reproduced with permission. Copyright 2014, Elsevier B.V.

um metal nanoparticle size and microwave skin depth[50–51]. In addition, the size of lithium metal particles can be analyzed based on the asymmetry of the EPR signal. Thus, EPR is a powerful tool for characterizing the microstructure of lithium metal. The EPR spectral quality factor, spin density, and changes in the EPR spectrum reflects the conductivity, degree of lithiation, and deposition process of graphite. Thus, the time-resolved and quantitative information obtained from operando EPR spectra is useful for optimizing fast-charging programs, electrolyte additive testing and model validation. *In-situ* EPR spectroscopy reveals that the lithium metal coating depends on the charging current during low-temperature (−20 °C) charging (Fig. 8a-c)[52]. Quantitative analysis of the EPR spectrum can quantify the amount of "dead lithium" and observe the chemical re-insertion of lithium metal. Line-shape analysis of EPR spectra can further distinguish the contributions of dead lithium and active lithium in the solid electrolyte interface (Fig. 8d-e). Wang et al.[53] designed a concentric-geometry three-electrode *in-situ* EPR cell with a metallic Li cathode wrapped with an Al current collector and a graphitic anode coated onto the inner copper wire to study the (de)lithiation of the LIB anode at room temperature. Only the graphite part was exposed to the EPR cavity to avoid the influence of the lithium counter/reference electrode and to highlight the weak graphite signal. The inner lithium reference electrode close to the graphite layer ensured an electrochemical performance equal to that of the coin cell. The MnO reference was used as the spin reference to monitor

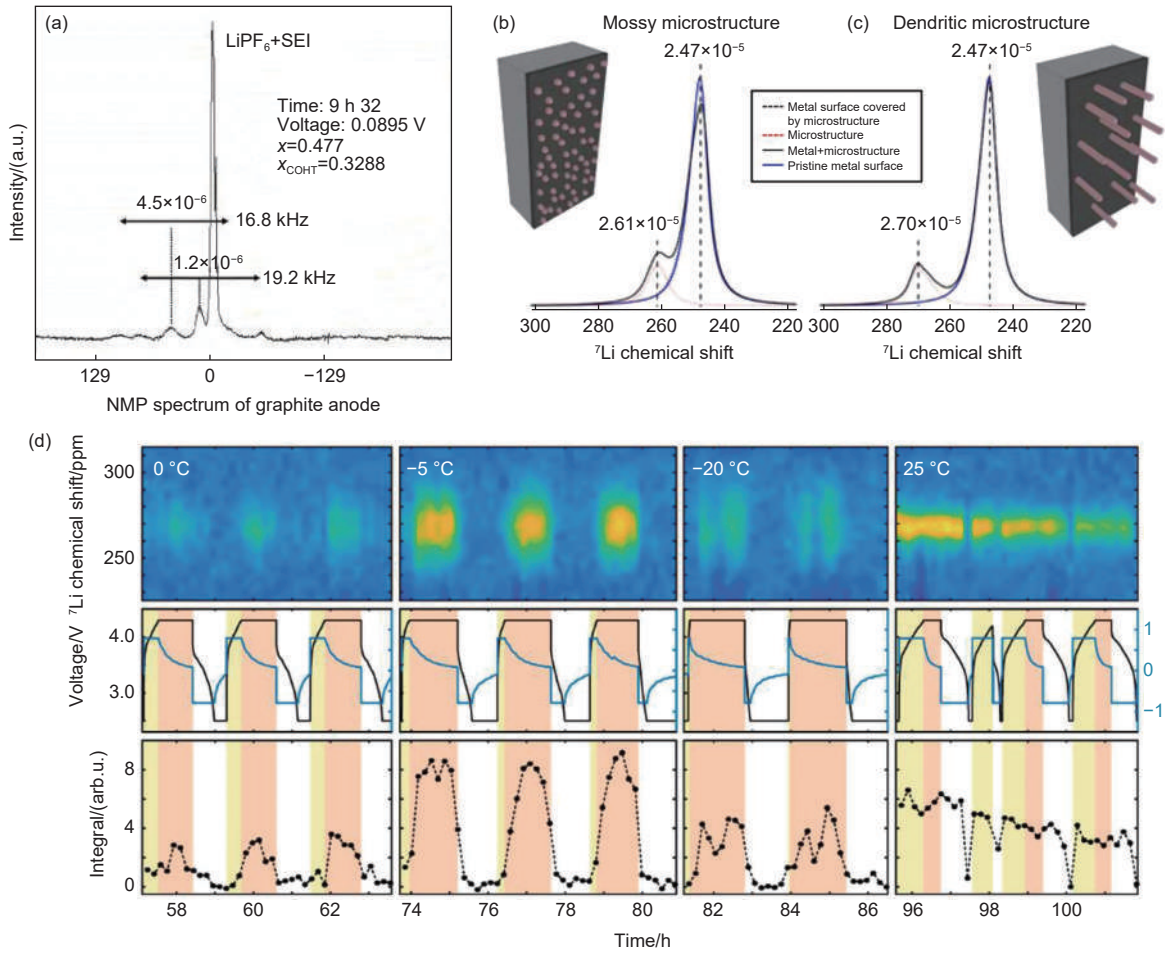

Fig. 7 (a) NMR spectrum of graphite anode during the first discharge[46]. Reproduced with permission. Copyright 2007, Elsevier Ltd. Simulated spectra from the FFT susceptibility calculation results for a lithium electrode with (b) a mossy type microstructure and (c) dendritic microstructure covering the surface[48]. Reproduced with permission. Copyright 2015, American Chemical Society. (d) Summary of the operando NMR results of NMC811/graphite full-cells operated at different temperatures: the lithium metal spectra at top panels, the corresponding voltage (black) and current (blue) profiles in middle and the lithium metal signal integral at bottom[49]. Reproduced with permission. Copyright 2020, American Chemical Society

the change in the EPR resonator quality factor. The *in-situ* results show that lithium metal deposition on the graphite anode does not require overcharging: lithium deposition begins at +0.04 V (*vs*. Li^+/Li) when the scan rate is reduced to 0.04 mV s^{-1}. The EPR results of the ethylene carbonate additive in the cycle process indicate that it has an inhibitory effect on lithium deposition, which is attributed to the flexible polymer SEI layer, which has a higher ion conductivity and can withstand greater mechanical stress caused by the insertion and extraction of lithium ions.

The combination of multiple techniques could enhance the comprehension of lithium deposition behavior. For example, Uhlmann et al.[54] employed pulse relaxation experiments, SEM and *in-situ* optical microscopy (Fig. 9a-b). To induce electrodeposition on the anode surface, current pulses up to 10 C were applied to the graphite half-cell. Characteristic features, such as changes in battery voltage and surface morphology, were analyzed during the pulse and subsequent relaxation periods. Several distinct attributes were detected whenever lithium deposition occurred: i) prominent kinks in voltage transients during charging, and ii) unique plateaus during subsequent battery voltage relaxation. These results were validated using models based on Butler-Volmer-type charge transfer and lithium diffusion in graphite grains. These findings were confirmed by the network-like structures covering the carbon particles observed in non-*in situ* SEM and the grey deposits covering the anode surface detected *in situ* optical microscopy.

Wang et al.[55] employed dynamic *in-situ* heating,

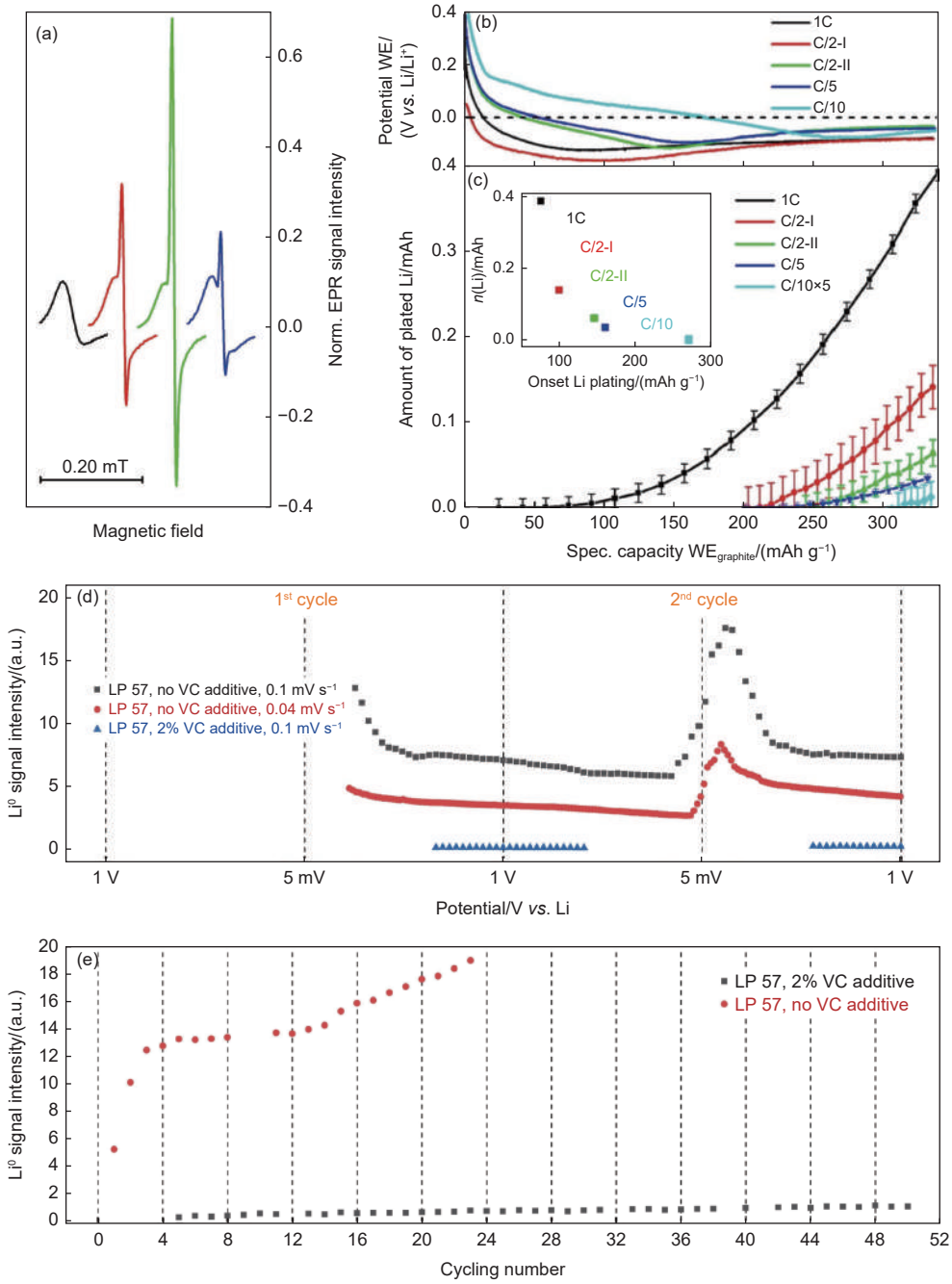

Fig. 8　(a) Selected EPR spectra, with spectra shown with an x-axis offset. (b) Potential curves of lithium intercalation at −20 °C at different C-rates. (c) Amount of metallic lithium as determined from operando EPR spectra as a function of intercalation capacity and applied C-rate[52]. Reproduced with permission. Copyright 2018, Elsevier Ltd. (d) The EPR intensity of metallic Li^0 deposition at graphite anode during the first two cycles with VC (blue) and without VC additive (black) at 0.1 mV s^{-1} and without VC at a lower scan rate of 0.04 mV s^{-1}; (e) Li^0 formation on the graphite surface during cycling from 0.05 to 1 V at 2 mV s^{-1}[53]. Reproduced with permission. Copyright 2021, Wiley-VCH GmbH

NMR, and finite element modeling to enhance the comprehension of the lithium deposition mechanism on graphite electrodes (Fig. 9c). Initially, they extracted the lithium electroplating signal from the graphite negative voltage and converted the unique lithium stripping plateau into an incremental capacity peak in the subsequent delithiation process. *In-situ* thermal spectra and additional heat peaks that corresponded to lithium stripping provided compelling evidence for lithium electroplating. During the lithiation and delithiation stages, signals of lithium deposition were extracted from the graphite voltage and increment capacity curves, with the delithiation plateau serving as a characteristic indicator of lithium deposition. The ad-

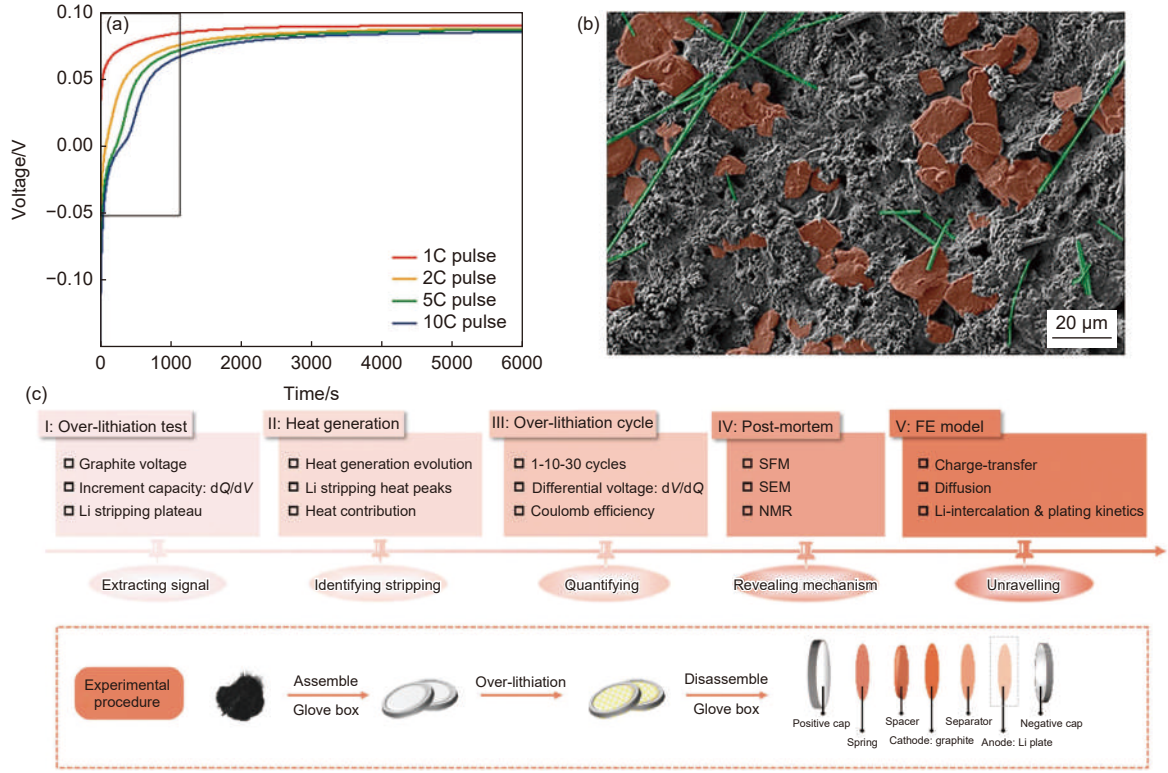

Fig. 9 (a) Measured voltage transients during the relaxation of the cell voltage after charging pulses with different current amplitudes. (b) SEM of the graphite anode cycled at C/5 for 5 times from 0.01 to 0.5 V. Graphite particles are marked red, the fibers (marked green) are separator remnants[54]. Reproduced with permission. Copyright 2015, Elsevier B.V. (c) Schematic diagram illustrating experimental and model approaches in understanding lithium plating synopsis[55]. Reproduced with permission. Copyright 2021, Elsevier B.V.

ditional heat peak confirmed the exothermic phenomenon during the delithiation process. As the lithiation increased from 100% SOC to 120% SOC, the total heat rose from 0.980 to 2.296 J due to the charging of additional capacity. Shortening the delithiation process weakened the initial exothermic reaction. In the cyclic process, longer lithium stripping plateaus were observed in comparison to the lithiation plateau, indicating a decrease in charging capacity with increasing cycle number due to the inevitable generation of "dead lithium."

4 Factors of suppressing lithium plating

The previous sections have provided a thorough overview of the electrochemical processes underlying lithium plating on graphite anode and the characterization methods used to observe and comprehend lithium deposition. Drawing on this knowledge, a variety of strategies have been developed to mitigate lithium plating which can be broadly classified into 3 categories: anode modification, electrolyte optimization and optimization of charging protocols. Anode modification is essential to improve the lithium transference capability, which can impact the growth of lithium dendrites. Electrolyte optimization aims to modify the composition or incorporate additives to prevent SEI damage and shield anode surface. Along with these internal factors, the manner in which the current changes during the battery charging process also exerts significant influence on the growth of lithium dendrites on the graphite surface[18, 27]. Therefore, optimizing charging protocols is an effective method for suppressing lithium plating.

4.1 Anode modification

For better comprehension of the different strategies, the characteristics of each strategy have been summarized in Table 1. Cai et al.[14] conducted a systematic investigation of the boundary of the graphite electrode with uniform lithium a conformal thin β-Poly(vinylidene fluoride) (β-PVDF) coating exhibits

dendrite-free lithium plating and maintains good cycling stability under any condition (e.g. 20% over-lithiation, fast lithiation at up to 10 C-rate)[56]. Another anode coating layer was developed which consists of carbon-coated porous titanium niobium oxides (TNO@C), where the relatively high voltage anode material titanium niobium oxides (TNO) could effectively avoid lithium dendrites under extreme conditions[57]. Tallman et al.[58] demonstrated an approach where a facile interfacial modification deliberately increases the overpotential for lithium metal deposition, providing a conceptual approach for suppressing lithium deposition on a graphite electrode. As shown in Fig. 10a, the metal coating increases the overpotential to prevent lithium from reaching the nucleation condition, thus reducing the nucleation site on the graphite surface of the metal coating, which could decrease the total quantity of lithium deposition. Compared with the cell that contains unmodified graphite, NMC622/Ni-coated graphite pouch cells exhibit excellent capacity retention which is approximate ~ 5% higher.

An approach to suppress lithium plating is to modify the structure of the anode, particularly by shorting the lithium diffusion path. Researchers have introduced defects to increase the chemical affinity to lithium deposition and expand storage capacity[59–60]. For example, reducing the particle size of graphite by ball milling creates micropores and surface defects that enhance the wettability between electrolyte and graphite, resulting in loose and small on the nature lithium surface but dense and smooth on the ball-milled graphite surface (Fig. 10b)[59]. Yeo et al.[60] grew defective carbon nanotubes defective carbon nanotube (dCNT) between nickel (Ni) particles and graphite to induce excessive and stable deposition of dense lithium with a smooth surface. In a full-cell test with a reverse-designed N/P ratio (0.8), the initial CE and discharge capacity of graphite (G), dCNT Graphite (dCNT-G), and double-layer electrode fabricated by casting dCNT-G slurry above dried G electrode (dCNT-G/G) for 300 cycles (0.3 C) are shown in Fig. 10c. The dCNT-G/G electrodes exhibited an initial CE of 87% and a boosted rate capacity with capacity retention of 83.5% after 300th cycle, which is superior to that of the graphite. However, the presence of defects can also be a disruptive factor that causes non-uniform ionic currents, leading to battery cell failure, despite a seemingly well-functioning and well-designed battery[61].

4.2 Electrolyte optimization

The effective design of electrolyte systems is critical to enhancing the lifetime, rate capability and safety of LIBs at present[62]. The stability of the SEI, a passivation film formed by the degradation of electrolyte salt and solvent, directly affects the electrochemical performances of batteries. To quantitatively research the relationship between the lithium deposition on the graphite electrode and the capacity loss, commercial 18650 $LiFePO_4$ (LFP)/graphite cells were cycled at 1 C rate to attain different capacity losses (5.7%, 9.2% and 15.8%) (Fig. 11a). It was found that the active lithium that causes the loss of capacity mostly deposit on the graphite surface, which is consumed by the rearrangement, repair and growth of SEI[63]. Thus, the stability and flexibility of SEI film on graphite anode are crucial, and electrolyte modification is a common strategy to improve its properties. McShane et al.[64] used a combination of differential electrochemical mass spectrometry (DEMS) and mass

Table 1　Anode modification methods of suppressing lithium plating

Anode modification	Material/Method	Advantages	Refs.
Anode coating layer	β-PVDF coating	(a) Mitigate lithium dendrite formation (b) Maintain good cycling stability with 20% over-lithiation at 0.2 C	[56]
	Carbon coated porous titanium niobium oxides	(a) Suppress lithium plating problem effectively under extreme fast charge condition (b) Deliver a high energy(142.8 Wh kg^{-1}) and a good energy retention	[57]
	DC magnetron sputtering of nanoscale layers of Cu and Ni	(a) Increase the overpotential for lithium deposition (b) Reduce the quantity of the plated lithium metal by ~ 50% compared to untreated electrodes	[58]
Anode structure modification	Ball milling	(a) Decrease the stress and strain upon co-intercalation of the solvated lithium ions (b) Integrate the structure and enhance the lithium plating/stripping cyclability of the graphite	[59]
	Defective carbon-nanotube-grown graphite	(a) Result in densely packed lithium deposition without any dendritic lithium plating (b) Remain electrochemically active even after 300 cycles	[60]

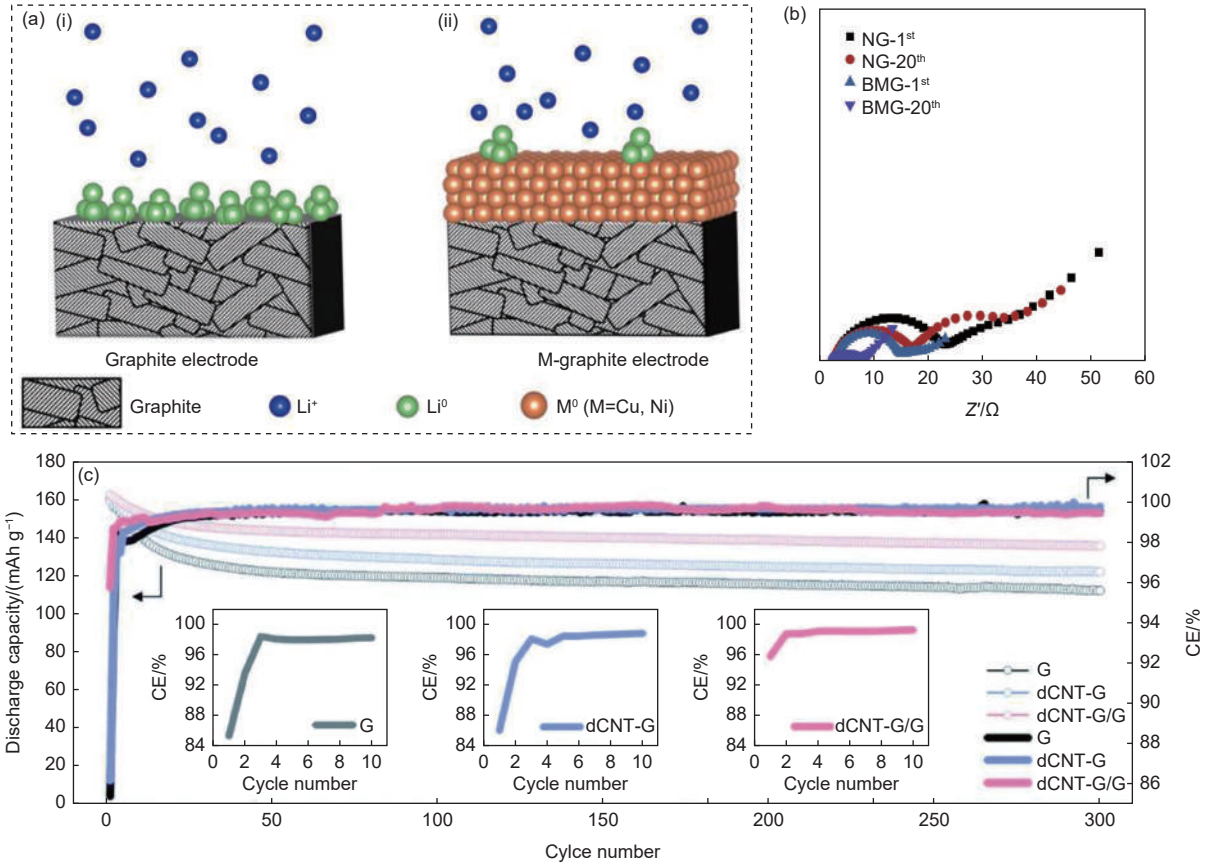

Fig. 10 (a) Schematic representation of (i) lithium metal nucleation on the graphite surface during high current charging and (ii) reduced nucleation due to increased overpotential for lithium metal deposition afforded by a Cu or Ni surface coating with a structural mismatch[58]. Reproduced with permission. Copyright 2019, American Chemical Society. (b) The impedance of natural graphite and ball-milling graphite after the first cycle and 20 cycles[59]. Reproduced with permission. Copyright 2019, Elsevier Ltd. (c) CE and discharge capacity of G, dCNT-G, and dCNT-G/G for 300 cycles (0.3 C)[60]. Reproduced with permission. Copyright 2022, Royal Society of Chemistry

spectrometric titration (MST) to quantify the graphite SEI components formed in electrolytes with different salt concentrations. The results showed that the overall SEI film became thinner with the increase of $LiPF_6$ concentration, and the SEI effect in 1.2 mol L^{-1} electrolyte was found to be the best in terms of capacity retention ability, despite the fact that the thinnest SEI film with the smallest resistance formed under 2.0 mol L^{-1} electrolyte. Thus, the research on electrolyte engineering should focus on the high concentration of electrolytes, while considering the SEI effect when exploring lithium plating behavior. The addition of lithium bis(fluorosulfonyl)imide (LiFSI) electrolyte to carbonate electrolyte can enhance the cycling performance of lithium deposited on graphite substrate. This is because the SEI film derived from FSI^- is dense and stable (Fig. 11b-c), which could protect the graphite substrate and hinder the co-intercalation of solvated ions in the process of lithium plating, thus preventing the electrolyte from reacting with the deposited lithium[65].

In addition to improving SEI properties, which can help prevent the dendrite formation, electrolytes can be designed with additives or modifications that specifically inhibit dendrite growth. The reducing compound formed by 1, 3-propane sultone as an electrolyte additive can cover the active sites of graphite, protecting the surface and inhibiting deposition of lithium metal[66]. The graphene oxide quantum dots (GOQD)-decorated a polymer framework comprising Poly(acrylonitrile-co-vinyl acetate) (PAV) and incorporated poly(methyl methacrylate) (PMMA) (PAVM) framework reduces ion-solvent clusters and the degree of lithium ion solvation to improve Li^+ transport in gel polymer electrolyte (GPE) (Fig. 11d-e), resulting in uniform deposition and stripping of lithium

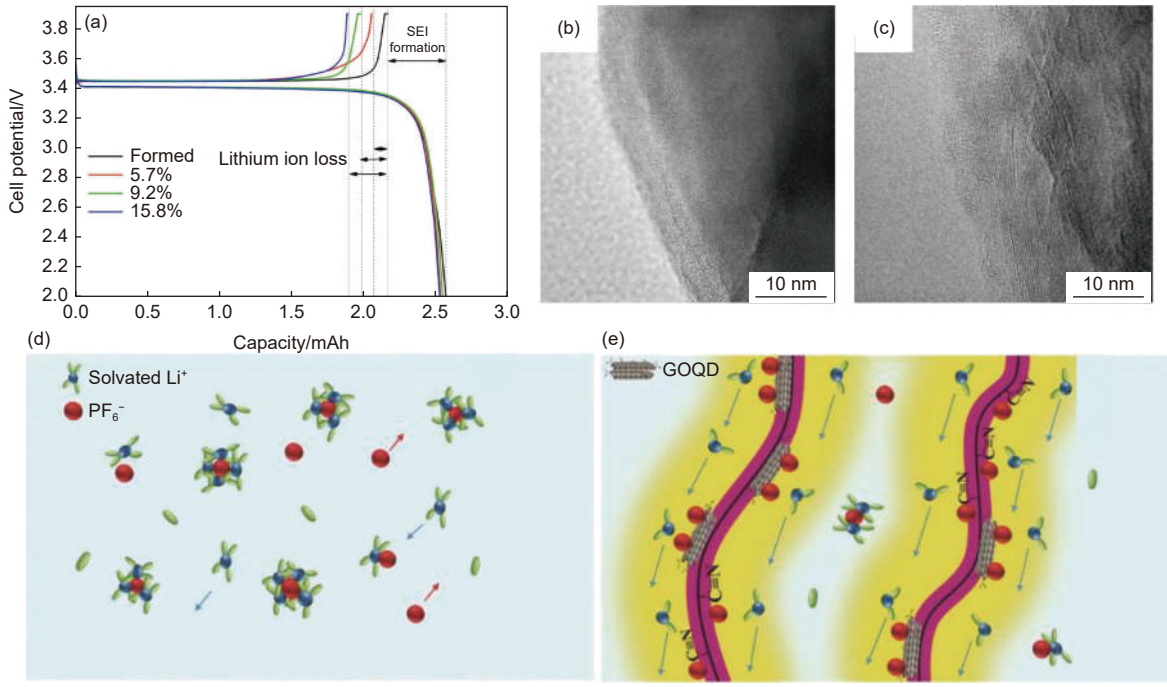

Fig. 11　(a) The first charge-discharge curves of the LFP electrodes harvested from the cycled cells with different capacity losses[63]. Reproduced with permission. Copyright 2015, Elsevier Ltd. TEM images of the graphite electrode charged to 0.1 V after 5 cycles of lithium plating/stripping in the (b) LiFSI and (c) $LiPF_6$ electrolyte[65]. Reproduced with permission. Copyright 2021, American Chemical Society. Conceptual illustrations of (d) liquid electrolyte which contains highly solvated lithium and ion-solvent clusters and (e) the GOQD-decorated polymer chains in GPE-PAVM: QD immobilize PF_6^- to minimize both the ion-solvent clusters and degree of lithium ion solvation, resulting formation of space-charge layers that facilitate the transport of lithium ions.[62]. Reproduced with permission. Copyright 2018, Wiley-VCH GmbH

metals[62]. These approaches demonstrate the potential for electrolyte design to play a key role in improving the lifetime, rate capability and safety of LIBs.

4.3　Optimization of charging protocols

Both the active material and electrolyte modifications have shown promising results, while most of them are complex, expensive and not feasible for mass production. As a result, many researchers have shifted their focus to seeking solutions from the cell and pack level. Charging strategy, which can determine the current variations during charging and simplify battery design, has garnered significant attention as a method that can be practically implemented. In optimizing the charging strategy, careful attention must be paid to the balance between fast charging and battery health to enhance the charging efficiency while ensuring battery safety[67]. In the following sections, we will examine the classic charging protocols and their characteristics, in addition to the optimization of charging protocols. Table 2 shows the advantages and disadvantages of various charging protocols.

The constant current constant voltage (CC/CV) charging protocol is widely used in commercial chargers due to its ease of use and implementation[68–69]. As shown in Fig. 12a, this protocol involves charging the battery at a constant current until it reaches the preset voltage at constant current, after which the voltage is held constant while continuing to charge until the current drops to the preset current, known as the CV stage[72]. However, the CC/CV high-rate charging method can easily trigger lithium plating. To address this issue, an improved method of the CC/CV charging protocol was investigated by utilizing a full cell comprised of the anode, cathode from 18650-type cells, and lithium metal reference electrode. Reducing the charge current in the standard CC/CV protocol can also enhance the cell's cyclability and total charge throughput, albeit at the cost of significantly longer charge times[27].

The multi-stage constant current (MSCC) charging protocol charges the battery using a sequence of stepwise descending currents, and has been proposed

Table 2 Advantages and disadvantages of charging protocols

Charging protocols	Method	Advantages	Disadvantages	Effect on lithium plating	Refs.
Constant current constant voltage (CC/CV)	Step1: CC-1 Step2: CC-2 Step3: CV-1	Simple, easy implementation, superior cycle life (over 5000 cycles)	Poor rate capacity, uncontrollable temperature	Determined by constant current and voltage	[68, 69]
Multi-stage constant current (MSCC/CV)	Step1: Multistage CC Step2: Multistage CC/CV Step3: Multistage CC Step4: CV	Short charging time, optimum battery performance, and thermal management	SOC needs to be estimated precisely, hard implementation	Limited effects	[68, 70]
Pulse charging	Nonlinearly decrease of charge current with the evolution of mass transfer coefficient	Reduced charging time, low polarization	Difficult to choose proper parameters for pulse sequence, easy to cause electrodes pulverization	Suspension of charge can inhibit lithium plating	[68, 71]
Boost charging	High pulse currents followed by CC/CV	Easy implementation, no impact on cycle life	Uncontrollable temperature, unoptimized charging rate	-	[68]

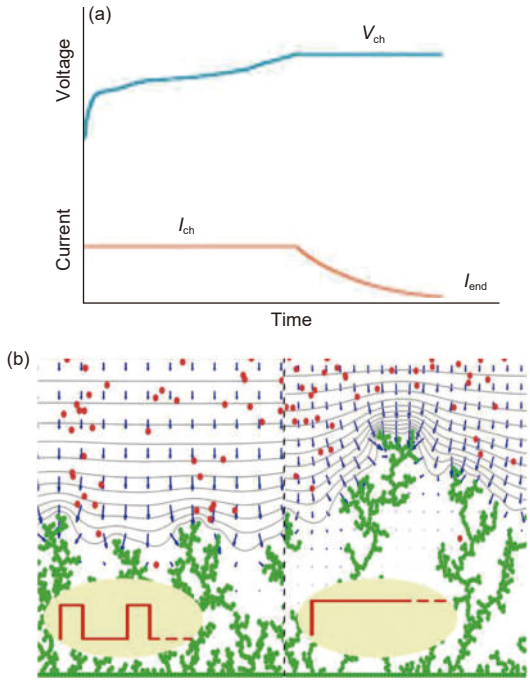

Fig. 12 (a) The voltage and the current plots under the CC/CV mode[72]. Reproduced with permission. Copyright 2016, Elsevier Ltd. (b) Simulations for charging with t_{ON} = 1 ms (left) and t_{ON} = 20 ms (right) at $\gamma = t_{OFF}/t_{ON}$ = 3. Green dots: Li^0. Red dots: Li. Gray lines: equipotential contours. Blue vectors: the electric field[71]. Reproduced with permission. Copyright 2014, American Chemical Society

as an alternative to the CC/CV charging protocol due to its ability of reducing polarization and lithium deposition[70]. Another variant of the CC/CV protocol is boost charging, in which the voltage initially rises to V_{max} for an initial period of t_0, and is then followed by a standard CC/CV strategy[73]. However, this protocol has limitations in terms of its ability to regulate temperature and optimize charging rates for the battery.

Pulse charging is a highly effective and rapid charging strategy for LIBs[22, 74–75], due to the rest time provided during the charging process which increases the diffusion efficiency of lithium ions in the electrode and reduces the polarization voltage[67]. This method improves energy efficiency and cyclic voltammogram characteristics in comparison to CC/CV charging[76]. A study by Aryanfar et al.[71] using Monte Carlo simulations to investigate the growth of lithium dendrites during pulse charging found that (Fig. 12b) a short charging time (1 ms) followed by a long relaxation time (3 ms) could effectively suppress lithium plating. However, the impact of temperature on pulse charging was not explored. Another study by Park and his colleagues[67] applied the battery model, which contained a degradation model, to pulse charging to determine the optimal pulse charging strategy. The results that longer rest times and lower temperature increases resulted in less degradation and temperature increases, and low temperatures were favorable for pulse charging. Moreover, further research is required to develop an integrated algorithm for applying pulse charging to commercial chargers.

4.4 Other approaches to suppressing Li plating

It is important to consider the role of thermodynamic factors in the growth of lithium dendrites in addition to the factors discussed. Temperature plays a crucial role in the equilibrium electrode potential of redox reactions, as temperature increases, so does the equilibrium potential of Li plating. Exothermic reaction and joule heat during cycling could raise the temperature of the cell, creating an internal temperature gradient that can intensify the thermal effect, especially at high-rate cycling[77]. Several experimental studies[78–81] have demonstrated that the temperature differences inside the battery could reach 2 K to nearly 30 K. This spatial variation in temperature results in a heterogeneous distribution of equilibrium po-

tentials between lithium plating and graphite intercalation on the anode, which may make lithium plating thermodynamically favorable in certain locations.

Wang et al.[82] established the correlation of the shift of the equilibrium potential of lithium plating and heterogeneous temperature distribution, demonstrating that metallic lithium can plate on a graphite anode above 0 V *vs*. Li^+/Li. Therefore, temperature heterogeneities within LIBs can cause lithium plating by altering its equilibrium electrode potential. Moreover, the metallic lithium may preferentially plate at high temperature regions under both slow and fast charging conditions. Hence, it is essential to maintain the homogeneous temperature within batteries for improving safety and cycle lifetime. To address the issue, Ge et al.[83] developed a temperature-adaptive alternating current heating method for LIB to ensure uniform temperature distribution. They used the temperature sensitivity of EIS to adjust the heating current parameters with the battery temperature during the heating process. This method considerably enhances the heating rate and lowers the danger of lithium plating.

5 Conclusion and perspective

LIBs that use graphite as their negative electrode are still the prevalent energy storage devices. However, the deposition of metallic lithium on the graphite surface is a severe side reaction that can lead to various problems, such as battery degradation, thermal runaway, short circuit and even explosion. In this review, we explore theoretical models and incorporate the latest characterization techniques to shed light on the factors influencing the impact of metallic lithium on the graphite surface. We also discuss strategies for suppressing this phenomenon.

Although the current theoretical models are relatively simple, developing new and more comprehensive models can aid in understanding the intricate dynamics of surface lithium-ion behavior. There is general agreement that Li deposition is influenced by the chemical and physical properties of the electrode, but there are still many unanswered questions about the exact nature of these interactions. For example, the role of defects, impurities, and surface functional groups on the graphite surface in controlling Li deposition is still not well understood.

Currently, fundamental research on lithium-ion batteries tends to focus on the three-electrode system, while the impact of the cathode material in practical applications cannot be ignored. Transition metal-based materials, which hold great promise as cathodes, have been shown to pose harm to the graphite anode via a series of processes[84–86]. However, those cathodes typically exhibit severe irreversible phase changes during cycling when operated at high C rate or high temperature, leading to the precipitation of metal ions. These ions can migrate and deposit on the surface of the graphite anode, serving as nucleation sites that further induce lithium metal deposition. Therefore, it is crucial to explore the influence of the cathode material on lithium deposition behavior in order to develop strategies to mitigate the issue[87–88].

Furthermore, there is a need to develop high-precision testing techniques that can detect the series of dynamic processes that occur on the graphite negative electrode in real batteries. For example, the higher-temporal-resolution Pulse EPR has shown its ability to track the transient process in a metallic lithium anode during fast charging, with a higher temporal resolution of 100 ms[89]. The SEI film, which plays a critical role in negative electrode performance, is challenging to characterize under operando conditions. Currently, techniques such as electrochemical scanning microscopy and atomic force microscopy can provide a mapping image of the SEI layer. However, long data collection times can distort information, and a faster but precise process is needed to address this issue. Methods such as SEI film pretreatment, the development of new electrolytes, and the use of more efficient electrolyte additives are effective approaches to tackle current challenges.

We hope that this review can offer valuable insights for researchers in relevant fields who are facing difficulties.

Acknowledgements

The authors acknowledge the financial support from the startup support grant from China University of Petroleum (East China) (27RA2204027), Shandong Provincial Natural Science Foundation (ZR2020ZD08), Taishan Scholars Program of Shandong Province (tsqn20221117), Shandong Province Postdoctoral Innovative Talent Support Program (SDBX2022034) and Qingdao Postdoctoral Innovation Project (QDBSH20220202003).

References

[1] Zhu Y L, Wang Y X, Gao C, et al. $CoMoO_4$-N-doped carbon hybrid nanoparticles loaded on a petroleum asphalt-based porous carbon for lithium storage[J]. New Carbon Materials, 2020, 35(4): 358-370.

[2] Wu M B, Li L Y, Liu J, et al. Template-free preparation of mesoporous carbon from rice husks for use in supercapacitors[J]. New Carbon Materials, 2015, 30(5): 471-475.

[3] Xia L, Yu L, Hu D, et al. Electrolytes for electrochemical energy storage[J]. Materials Chemistry Frontiers, 2017, 1(4): 584-618.

[4] Guan L, Hu H, Teng X L, et al. Templating synthesis of porous carbons for energy-related applications: A review[J]. New Carbon Materials, 2022, 37(1): 25-45.

[5] Moharana S, West G, Walker M, et al. Controlling Li dendritic growth in graphite anodes by potassium electrolyte additives for Li-ion batteries[J]. ACS Applied Materials & Interfaces, 2022, 14(37): 42078-42092.

[6] Armand M, Tarascon J M. Building better batteries[J]. Nature, 2008, 451(7179): 652-657.

[7] Goodenough J B, Park K S. The Li-ion rechargeable battery: A perspective[J]. Journal of the American Chemical Society, 2013, 135(4): 1167-1176.

[8] Etacheri V, Marom R, Elazari R, et al. Challenges in the development of advanced Li-ion batteries: a review[J]. Energy & Environmental Science, 2011, 4(9): 3243-3262.

[9] Palacín M R, de Guibert A. Why do batteries fail [J]? Science, 2016, 351(6273): 1253292.

[10] Wang X, Huang R Q, Niu S Z, et al. Research progress on graphene-based materials for high-performance lithium-metal batteries[J]. New Carbon Materials, 2021, 36(4): 711-728.

[11] Fang R, Chen K, Yin L, et al. The regulating role of carbon nanotubes and graphene in lithium-Ion and lithium –sulfur batteries[J]. Advanced Materials, 2019, 31(9): 1800863.

[12] Wakihara M. Recent developments in lithium ion batteries[J]. Materials Science and Engineering:R:Reports, 2001, 33(4): 109-134.

[13] Ecker M, Shafiei Sabet P, Sauer D U. Influence of operational condition on lithium plating for commercial lithium-ion batteries[J]. Electrochemical experiments and post-mortem-analysis. Applied Energy, 2017, 206: 934-946.

[14] Cai W, Yan C, Yao Y X, et al. The boundary of lithium plating in graphite electrode for safe lithium-Ion batteries[J]. Angewandte Chemie International Edition, 2021, 60(23): 13007-13012.

[15] Lu J, Chen Z, Pan F, et al. High-performance anode materials for rechargeable lithium-ion batteries[J]. Electrochemical Energy Reviews, 2018, 1(1): 35-53.

[16] Waldmann T, Hogg B I, Wohlfahrt-Mehrens M. Li plating as unwanted side reaction in commercial Li-ion cells- a review[J]. Journal of Power Sources, 2018, 384: 107-124.

[17] Liu Q, Du C, Shen B, et al. Understanding undesirable anode lithium plating issues in lithium-ion batteries[J]. RSC Advances, 2016, 6(91): 88683-88700.

[18] Li Z, Huang J, Yann Liaw B, et al. A review of lithium deposition in lithium-ion and lithium metal secondary batteries[J]. Journal of Power Sources, 2014, 254: 168-182.

[19] Aurbach D, Zinigrad E, Cohen Y, et al. A short review of failure mechanisms of lithium metal and lithiated graphite anodes in liquid electrolyte solutions[J]. Solid State Ionics, 2002, 148(3): 405-416.

[20] Persson K, Sethuraman V A, Hardwick L J, et al. Lithium diffusion in graphitic carbon[J]. The Journal of Physical Chemistry Letters, 2010, 1(8): 1176-1180.

[21] Legrand N, Knosp B, Desprez P, et al. Physical characterization of the charging process of a Li-ion battery and prediction of Li plating by electrochemical modelling[J]. Journal of Power Sources, 2014, 245: 208-216.

[22] Purushothaman B K, Landau U. Rapid charging of lithium-ion batteries using pulsed currents: A theoretical analysis[J]. Journal of The Electrochemical Society, 2006, 153(3): A533.

[23] Arora P, Doyle M, White R E. Mathematical modeling of the lithium deposition overcharge reaction in lithium-Ion batteries using carbon-based negative electrodes[J]. Journal of The Electrochemical Society, 1999, 146(10): 3543.

[24] Tang M, Albertus P, Newman J. Two-dimensional modeling of lithium deposition during cell charging[J]. Journal of The Electrochemical Society, 2009, 156(5): A390.

[25] Perkins R D, Randall A V, Zhang X, et al. Controls oriented reduced order modeling of lithium deposition on overcharge[J]. Journal of Power Sources, 2012, 209: 318-325.

[26] Hein S, Latz A. Influence of local lithium metal deposition in 3D microstructures on local and global behavior of lithium-ion batteries[J]. Electrochimica Acta, 2016, 201: 354-365.

[27] Waldmann T, Kasper M, Wohlfahrt-Mehrens M. Optimization of charging strategy by prevention of lithium deposition on anodes in high-energy lithium-ion batteries[J]. Electrochemical Experiments. Electrochimica Acta, 2015, 178: 525-532.

[28] Liu S, Xiong L, He C. Long cycle life lithium ion battery with lithium nickel cobalt manganese oxide (NCM) cathode[J]. Journal of Power Sources, 2014, 261: 285-291.

[29] Waldmann T, Hogg B-I, Kasper M, et al. Interplay of operational

parameters on lithium deposition in lithium-ion cells: systematic measurements with reconstructed 3-electrode pouch full cells[J]. Journal of The Electrochemical Society, 2016, 163(7): A1232.

[30] Bugga R V, Smart M C. Lithium plating behavior in lithium-ion cells[J]. ECS Transactions, 2010, 25(36): 241.

[31] Waldmann T, Wilka M, Kasper M, et al. Temperature dependent ageing mechanisms in lithium-ion batteries: A post-mortem study[J]. Journal of Power Sources, 2014, 262: 129-135.

[32] Blyr A, Sigala C, Amatucci G, et al. Self-discharge of $LiMn_2O_4$/C Li - ion cells in their discharged state: understanding by means of three - electrode measurements[J]. Journal of The Electrochemical Society, 1998, 145(1): 194.

[33] Lin H P, Chua D, Salomon M, et al. Low-temperature behavior of Li-ion cells[J]. Electrochemical and Solid-State Letters, 2001, 4(6): A71.

[34] Zhang S S, Xu K, Jow T R. Study of the charging process of a $LiCoO_2$-based Li-ion battery[J]. Journal of Power Sources, 2006, 160(2): 1349-1354.

[35] Petzl M, Danzer M A. Nondestructive detection, characterization, and quantification of lithium plating in commercial lithium-ion batteries[J]. Journal of Power Sources, 2014, 254: 80-87.

[36] Konz Z M, McShane E J, McCloskey B D. Detecting the onset of lithium plating and monitoring fast charging performance with voltage relaxation[J]. ACS Energy Letters, 2020, 5(6): 1750-1757.

[37] Ho A S, Parkinson D Y, Finegan D P, et al. 3D detection of lithiation and lithium plating in graphite anodes during fast charging[J]. ACS Nano, 2021, 15(6): 10480-10487.

[38] Harris S J, Timmons A, Baker D R, et al. Direct in situ measurements of Li transport in Li-ion battery negative electrodes[J]. Chemical Physics Letters, 2010, 485(4): 265-274.

[39] Dahn J R. Phase diagram of Li_xC_6[J]. Physical Review B, 1991, 44(17): 9170-9177.

[40] Gao T, Han Y, Fraggedakis D, et al. Interplay of lithium intercalation and plating on a single graphite particle[J]. Joule, 2021, 5(2): 393-414.

[41] Downie L E, Krause L J, Burns J C, et al. In situ detection of lithium plating on graphite electrodes by electrochemical calorimetry[J]. Journal of The Electrochemical Society, 2013, 160(4): A588.

[42] Birkenmaier C, Bitzer B, Harzheim M, et al. Lithium plating on graphite negative electrodes: Innovative qualitative and quantitative investigation methods[J]. Journal of The Electrochemical Society, 2015, 162(14): A2646.

[43] Bommier C, Chang W, Lu Y, et al. In operando acoustic detection of lithium metal plating in commercial $LiCoO_2$/graphite pouch cells[J]. Cell Reports Physical Science, 2020, 1(4): 100035.

[44] Avdeev M V, Rulev A A, Bodnarchuk V I, et al. Monitoring of lithium plating by neutron reflectometry[J]. Applied Surface Science, 2017, 424: 378-382.

[45] Veronika Z, Christian V L, Michael H, et al. Lithium plating in lithium-ion batteries at sub-ambient temperatures investigated by in situ neutron diffraction[J]. Journal of Power Sources, 2014, 271: 152-159.

[46] Letellier M, Chevallier F, Morcrette M. In situ 7Li nuclear magnetic resonance observation of the electrochemical intercalation of lithium in graphite; 1st cycle[J]. Carbon, 2007, 45(5): 1025-1034.

[47] Börner M, Friesen A, Grützke M, et al. Correlation of aging and thermal stability of commercial 18650-type lithium ion batteries[J]. Journal of Power Sources, 2017, 342: 382-392.

[48] Chang H J, Trease N M, Ilott A J, et al. Investigating Li microstructure formation on Li anodes for lithium batteries by in situ $^6Li/^7Li$ NMR and SEM[J]. The Journal of Physical Chemistry C, 2015, 119(29): 16443-16451.

[49] Märker K, Xu C, Grey C P. Operando NMR of NMC811/graphite lithium-ion batteries: Structure, dynamics, and lithium metal deposition[J]. Journal of the American Chemical Society, 2020, 142(41): 17447-17456.

[50] Niemöller A, Jakes P, Eichel R-A, et al. EPR Imaging of metallic lithium and its application to dendrite localisation in battery separators[J]. Scientific Reports, 2018, 8(1): 14331.

[51] Pifer J H, Magno R. Conduction-electron spin resonance in a lithium film[J]. Physical Review B, 1971, 3(3): 663-673.

[52] Wandt J, Jakes P, Granwehr J, et al. Quantitative and time-resolved detection of lithium plating on graphite anodes in lithium ion batteries[J]. Materials Today, 2018, 21(3): 231-240.

[53] Wang B, Le Fevre L W, Brookfield A, et al. Resolution of lithium deposition versus intercalation of graphite anodes in lithium ion batteries: an in situ electron paramagnetic resonance study[J]. Angewandte Chemie International Edition, 2021, 60(40): 21860-21867.

[54] Uhlmann C, Illig J, Ender M, et al. In situ detection of lithium metal plating on graphite in experimental cells[J]. Journal of Power Sources, 2015, 279: 428-438.

[55] Mei W, Jiang L, Liang C, et al. Understanding of Li-plating on graphite electrode: Detection, quantification and mechanism revelation[J]. Energy Storage Materials, 2021, 41: 209-221.

[56] Luo J, Wu C E, Su L Y, et al. A proof-of-concept graphite anode with a lithium dendrite suppressing polymer coating[J]. Journal of Power Sources, 2018, 406: 63-69.

[57] Lyu H, Li J, Wang T, et al. Carbon coated porous titanium niobium oxides as anode materials of lithium-ion batteries for extreme fast charge applications[J]. ACS Applied Energy Materials, 2020, 3(6): 5657-5665.

[58] Tallman K R, Zhang B, Wang L, et al. Anode overpotential control via interfacial modification: Inhibition of lithium plating on graphite anodes[J]. ACS Applied Materials & Interfaces, 2019, 11(50): 46864-46874.

[59] Yang G, Zhang S, Tong Y, et al. Minimizing carbon particle size to improve lithium deposition on natural graphite[J]. Carbon, 2019,

155: 9-15.

[60] Yeo G, Sung J, Choi M, et al. Dendrite-free lithium deposition on conventional graphite anode by growth of defective carbon-nanotube for lithium-metal/ion hybrid batteries[J]. Journal of Materials Chemistry A, 2022, 10(24): 12938-12945.

[61] Cannarella J, Arnold C B. The effects of defects on localized plating in lithium-ion batteries[J]. Journal of The Electrochemical Society, 2015, 162(7): A1365.

[62] Chen Y M, Hsu S T, Tseng Y H, et al. Minimization of ion-solvent clusters in gel electrolytes containing graphene oxide quantum dots for lithium-ion batteries[J]. Small, 2018, 14(12): 1703571.

[63] Zheng H, Tan L, Zhang L, et al. Correlation between lithium deposition on graphite electrode and the capacity loss for $LiFePO_4$/graphite cells[J]. Electrochimica Acta, 2015, 173: 323-330.

[64] McShane E J, Bergstrom H K, Weddle P J, et al. Quantifying graphite solid-Electrolyte interphase chemistry and its impact on fast charging[J]. ACS Energy Letters, 2022, 7(8): 2734-2744.

[65] Yang G, Zhang S, Weng S, et al. Anionic effect on enhancing the stability of a solid electrolyte interphase film for lithium deposition on graphite[J]. Nano Letters, 2021, 21(12): 5316-5323.

[66] Park G, Nakamura H, Lee Y, et al. The important role of additives for improved lithium ion battery safety[J]. Journal of Power Sources, 2009, 189(1): 602-606.

[67] Park T R, Lee J I, Choi Y S. Investigation on optimal pulse current charging of lithium-ion batteries using electro-chemical model [C]. 2021 21st International Conference on Control, Automation and Systems (ICCAS), 2021, 978-1-6654-1832-4, 2642-3901.

[68] Gao Y, Zhang X, Cheng Q, et al. Classification and review of the charging strategies for commercial lithium-ion batteries[J]. IEEE Access, 2019, 7: 43511-43524.

[69] Spingler F B, Wittmann W, Sturm J, et al. Optimum fast charging of lithium-ion pouch cells based on local volume expansion criteria[J]. Journal of Power Sources, 2018, 393: 152-160.

[70] Anseán D, González M, Viera J C, et al. Fast charging technique for high power lithium iron phosphate batteries: a cycle life analysis[J]. Journal of Power Sources, 2013, 239: 9-15.

[71] Aryanfar A, Brooks D, Merinov B V, et al. Dynamics of lithium dendrite growth and inhibition: pulse charging experiments and monte carlo calculations[J]. The Journal of Physical Chemistry Letters, 2014, 5(10): 1721-1726.

[72] Peter K, Andreas J, Charging protocols for lithium-ion batteries and their impact on cycle life—an experimental study with different 18650 high-power cells[J], Journal of Energy Storage, 2016, 6: 125-141.

[73] Notten P H L, Veld J H G O h, Beek J R G v. Boostcharging Li-ion batteries: a challenging new charging concept[J]. Journal of Power Sources, 2005, 145(1): 89-94.

[74] Amanor-Boadu J M, Guiseppi-Elie A, Sánchez-Sinencio E. The impact of pulse charging parameters on the life cycle of lithium-ion polymer batteries[J]. Energies, 2018, 11(8): 11082162.

[75] Smith K, Wang C Y. Solid-state Diffusion limitations on pulse operation of a lithium ion cell for hybrid electric vehicles[J]. Journal of Power Sources, 2006, 161(1): 628-639.

[76] Li J, Murphy E, Winnick J, et al. The effects of pulse charging on cycling characteristics of commercial lithium-ion batteries[J]. Journal of Power Sources, 2001, 102(1): 302-309.

[77] Bandhauer T M, Garimella S, Fuller T F. A critical review of thermal issues in lithium-ion batteries[J]. Journal of The Electrochemical Society, 2011, 158(3): R1.

[78] Onda K, Ohshima T, Nakayama M, et al. Thermal behavior of small lithium-ion battery during rapid charge and discharge cycles[J]. Journal of Power Sources, 2006, 158(1): 535-542.

[79] Zhang G, Cao L, Ge S, et al. In situ measurement of radial temperature distributions in cylindrical Li-ion cells[J]. Journal of The Electrochemical Society, 2014, 161(10): A1499.

[80] Onda K, Kameyama H, Hanamoto T, et al. Experimental study on heat generation behavior of small lithium-ion secondary batteries[J]. Journal of The Electrochemical Society, 2003, 150(3): A285.

[81] Lee C Y, Lee S J, Tang M S, et al. In situ monitoring of temperature inside lithium-ion batteries by flexible micro temperature sensors[J]. Sensors, 2011, 11(10): 9942-9950.

[82] Wang H, Zhu Y, Kim S C, et al. Underpotential lithium plating on graphite anodes caused by temperature heterogeneity[J]. Proceedings of the National Academy of Sciences, 2020, 117(47): 29453-29461.

[83] Ge H, Huang J, Zhang J, et al. Temperature-adaptive alternating current preheating of lithium-ion batteries with lithium deposition prevention[J]. Journal of The Electrochemical Society, 2016, 163(2): A290.

[84] Langdon J, Manthiram A. Crossover effects in batteries with high-nickel cathodes and lithium-metal anodes[J]. Advanced Functional Materials, 2021, 31: 2010267.

[85] Choi J, Aurbach D. Promise and reality of post-lithium-ion batteries with high energy densities[J]. Nature Reviews Materials, 2016, 1: 16013.

[86] Li M, Lu J, Chen Z, et al. 30 years of lithium-ion batteries[J]. Advanced Materials, 2018, 30: 1800561.

[87] Li B, Wang Y Q, Lin H B, et al. Improving high voltage stability of lithium cobalt oxide/graphite battery via forming protective films simultaneously on anode and cathode by using electrolyte additive[J]. Electrochimica Acta, 2014, 141: 263-270.

[88] Li W S. Review—an unpredictable hazard in lithium-ion batteries from transition metal ions: dissolution from cathodes[J]. Deposition on Anodes and Elimination Strategies. Journal of The Electrochemical Society, 2020, 167: 090514.

[89] Szczuka C, Ackermann J, Schleker P P M, et al. Transient morphology of lithium anodes in batteries monitored by in operando pulse electron paramagnetic resonance[J]. Communications Materials, 2021, 2: 20.